



for geotechnics & structures

NUMERICAL SIMULATION OF FAILURE IN ELASTOPLASTIC LAYERED MEDIA THEORY AND APPLICATIONS

Report 070404

**Stéphane Commend
Th. Zimmermann
A. Truty**

GeoDev.

PO Box CH-1001 Lausanne
Switzerland
<https://zsoil.com>

Contents

1	Introduction	3
2	Constitutive model	5
2.1	Menétrey-Willam model	5
2.2	Multilaminate model	6
3	Simple Benchmarks Problems	9
3.1	One element test, one set of joints, 2D case	9
3.2	One element test, two sets of joints, 3D case	12
4	Applications	15
4.1	Cuts and slopes	15
4.1.1	Multilaminate vertical cut	15
4.1.2	Vertical cut with two layers of material	16
4.1.3	Slope stability with two sets of joints	17
4.2	Circular hole	18
5	Conclusion	21

Chapter 1

Introduction

Soils and rocks sometimes show preferential directions of weakness planes. In order to take into account these features in failure simulation, a constitutive model combining a multilaminate model with three possible lamina directions [1], to simulate the weakness planes, and a general three-parameters yield surface [2], to simulate the soil matrix, is proposed. The constitutive model theory is first reviewed, followed by two single-element benchmark problems treated with ZTunnel_3D in order to validate the model. Finally, case studies involving failures of cuts and circular holes are presented.

Chapter 2

Constitutive model

2.1 Menétrey-Willam model

Failure running across the preexisting weakness planes is governed by the Menétrey-Willam criterion [2]. This three-parameters yield surface can be formulated as follows:

$$F(x, r, q) = [Ar]^2 + m[Brr(q, e) + Cx] - 1 = 0$$

with:

$$r(q, e) = \frac{4(1 - e^2) \cos^2 q + (2e - 1)^2}{2(1 - e^2) \cos q + (2e - 1)[4(1 - e^2) \cos^2 q + 5e^2 - 4e]^{1/2}}$$

and invariants:

$$\begin{aligned} \xi &= \frac{1}{\sqrt{3}} I_1; & I_1 &= \sigma_{ii} = \sigma_1 + \sigma_2 + \sigma_3 \\ \rho &= \sqrt{2J_2}; & J_2 &= \frac{1}{2} S_{ij} S_{ij} = \frac{1}{2} \sum (\sigma_i - \sigma_m) \\ \cos 3\theta &= \frac{3\sqrt{3}}{2} \frac{J_3}{J_2^{3/2}}; & J_3 &= \frac{1}{3} S_{ij} S_{jk} S_{ki} \end{aligned}$$

θ is Lode's angle and A, B, C, m are parameters function of f_t the uniaxial tensile strength, f_c the uniaxial compressive strength and e the exentricity. The MW criterion can be specialized to a number of classical criteria, as illustrated next.

Alternative definitions of the Menétrey-Willam parameters are also possible using c and ϕ , the soil's cohesion and friction angle, or k and a_ϕ , the Drucker-Prager material parameters (see Table 2).

Table 2.1: Menétrey-Willam parameters

Generalized criterion	A	B	C	m	e
Huber-Misès	0	$\sqrt{\frac{3}{2}} \frac{1}{f_c}$	0	1	1
Drucker-Prager	0	$\sqrt{\frac{3}{8}} \frac{f_c + f_t}{f_c f_t}$	$\frac{3}{2} \frac{f_c - f_t}{f_c f_t}$	1	1
Rankine	0	$\frac{1}{\sqrt{6} f_t}$	$\frac{1}{\sqrt{3} f_t}$	1	$\frac{1}{2}$
Mohr-Coulomb (smooth)	0	$\frac{1}{\sqrt{6}} \frac{f_c + 2f_t}{f_c f_t}$	$\frac{1}{\sqrt{3}} \frac{f_c - f_t}{f_c f_t}$	1	$\frac{f_c + 2f_t}{2f_c + f_t}$
Hoek-Brown (smooth)	$\frac{\sqrt{1.5}}{f_c}$	$\frac{1}{\sqrt{6} f_c}$	$\frac{1}{\sqrt{3} f_c}$	$3 \frac{f_c^2 - f_t^2}{f_c f_t} \frac{e}{e + 1}$	e

Table 2.2: Menétrey-Willam parameters (alternative definition)

Generalized criterion	A	B	C	m	e
Huber-Misès	0	$\frac{1}{\sqrt{2}k}$	0	1	1
Drucker-Prager	0	$\frac{1}{\sqrt{2}k}$	$\sqrt{3} \frac{a_\phi}{k}$	1	1
Mohr-Coulomb (smooth)	0	$\frac{3 - \sin \phi}{\sqrt{24}c \cos \phi}$	$\frac{1}{\sqrt{3}c} \tan \phi$	1	$\frac{3 - \sin \phi}{3 + \sin \phi}$

2.2 Multilaminate model

One to three weakness planes orientations can be introduced, which will remain fixed in space. Each is characterized by a cohesion c_i , a friction angle ϕ_i and a dilatancy (non-associated) angle ψ_i (like any Coulomb type material). A tensile cut-off can be specified with f_{ti} the maximum tensile stress.

On each plane separately, the Mohr-Coulomb plasticity condition and the tension cut-off condition must be fulfilled.

Plasticity and flow rule conditions can be derived for each plane $i = 1, \dots, 3$:

$$\begin{aligned}
 F_{(1i)} &= \tau + \sigma_n \tan \phi_i - c_i \\
 F_{(2i)} &= -\tau + \sigma_n \tan \phi_i - c_i \\
 F_{(3i)} &= \sigma_n - f_{ti}
 \end{aligned} \tag{2.1}$$

$$\begin{aligned}
 G_{(1i)} &= \tau + \sigma_n \tan \psi_i - c_i \\
 G_{(2i)} &= -\tau + \sigma_n \tan \psi_i - c_i \\
 G_{(3i)} &= \sigma_n - f_{ti}
 \end{aligned} \tag{2.2}$$

$\hat{\sigma}_i$ represents the stress components in the i -th weakness plane (denoted by α_i):

$$\hat{\sigma}_i = \underline{T}_i : \underline{\sigma}$$

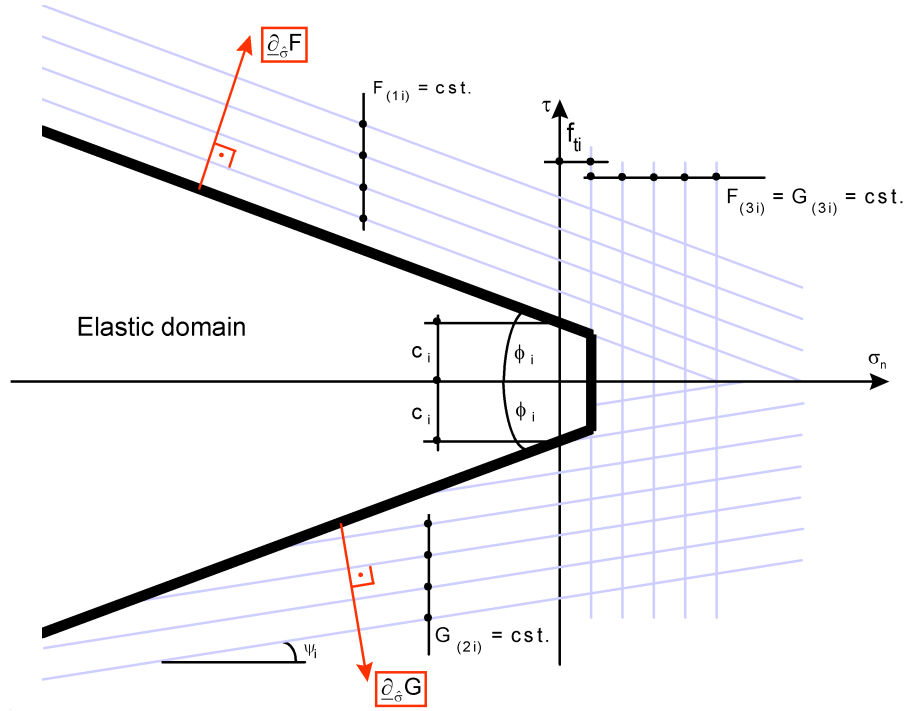


Figure 2.1: Weakness plane plasticity conditions, yield function & flow potential isolines

with:

$$\hat{\underline{\sigma}}_i = \begin{bmatrix} \sigma_n \\ \tau \end{bmatrix}^i \quad \underline{\sigma} = \begin{bmatrix} \sigma_x \\ \sigma_y \\ \tau_{xy} \end{bmatrix} \quad \underline{T}_i = \begin{bmatrix} s^2 & c^2 & -2sc \\ -sc & sc & c^2 - s^2 \end{bmatrix}^i$$

where

$$s = \sin \alpha_i, \quad c = \cos \alpha_i$$

This leads to a multisurface plasticity problem which requires that plasticity conditions (2.1) must be simultaneously fulfilled by any stress state in the material.

The flow rule is governed by a flow potential G (see (2.2)). As a dilatancy angle ψ^i is introduced for each plane; as it can differ from the friction angle ϕ^i , the flow rule adopted is usually non-associative ($G_i \neq F_i$).

Plastic strains occur due to violation of any of these plastic conditions by the elastic trial stress. The total plastic strain is the sum of each plane's contribution:

$$\begin{aligned} \dot{\underline{\varepsilon}}_i^p &= \dot{g}_i \partial_{\underline{\sigma}} G_i \\ \dot{\underline{\varepsilon}}^p &= \sum_i \dot{\underline{\varepsilon}}_i^p \end{aligned}$$

A perfectly elastic-plastic behavior (no hardening) is assumed.

This leads to the following constitutive equations for the multilaminate model:

$$\begin{aligned} \underline{\sigma} &= \underline{D} : (\underline{\varepsilon} - \underline{\varepsilon}^p) \\ \dot{\underline{\varepsilon}}^p &= \sum_i \dot{g}_i \partial_{\underline{\sigma}} G_i \end{aligned}$$

with the yield and (un)loading conditions for each plane $i = 1, \dots, 3$:

$$\begin{aligned}\dot{g}_i &\geq 0 \\ F_i(\underline{\sigma}) &\leq 0 \\ \dot{g}_i F_i(\underline{\sigma}) &= 0 \\ \dot{g}_i \dot{F}_i(\underline{\sigma}) &= 0\end{aligned}$$

In expanded form:

$$\begin{aligned}F_i(\underline{\sigma}) &\leq 0 \text{ and } \dot{F}_i(\underline{\sigma}) < 0 \quad \Rightarrow \quad \dot{g}_i = 0 \\ F_i(\underline{\sigma}) &= 0 \text{ and } \dot{F}_i(\underline{\sigma}) = 0 \quad \Rightarrow \quad \dot{g}_i > 0 \text{ (in this case the } i\text{-th plane constraint is **active**)}.\end{aligned}$$

Chapter 3

Simple Benchmarks Problems

3.1 One element test, one set of joints, 2D case

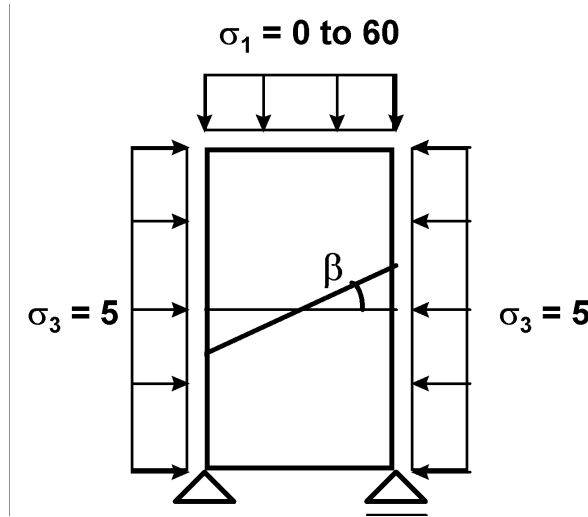


Figure 3.1: One element 2D test, geometry and loading

Rock characteristics: $c_r = 10$ [kN/m²], $\phi_r = 30^\circ$ (Drucker-Prager specialization of MW, external size-adjustment)

Joint characteristics: $c_j = 5$ [kN/m²], $\phi_j = 20^\circ$, $\psi_j = 0.66\phi_j = 13.33^\circ$

Note: σ_2 (in the transverse direction) is initially set to 5 [kN/m²]. It then evolves but remains between σ_3 and σ_1 . This leads to the conclusion that the $\sigma_3 - \sigma_1$ Mohr circle is the critical Mohr circle.

A first analysis is performed without the presence of the set of joints (rock only). This gives an ultimate load of:

$$\sigma_{1rf} = 50[\text{kN/m}^2]$$

This corresponds to the value of σ_1 for which the $\sigma_3 - \sigma_1$ Mohr circle is tangent to the Mohr-Coulomb law defined by $c_r = 10$ [kN/m²] and $\phi_r = 30^\circ$.

Then, one set of joint is added to the model, with a varying inclination angle of $0^\circ \leq \beta \leq 90^\circ$. Between two limit angles β_{\min} and β_{\max} , the failure will occur in the lamina. Outside of this

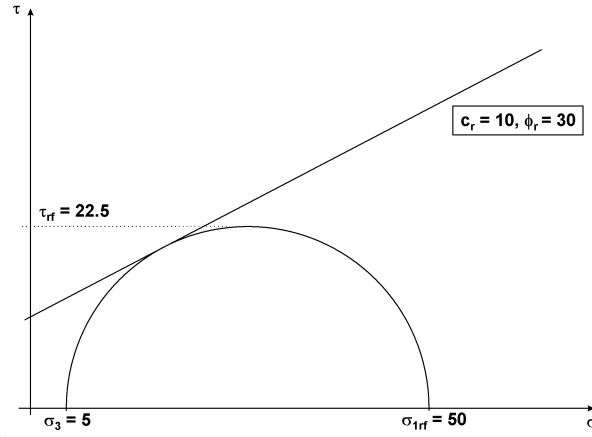


Figure 3.2: Mohr circle for the “rock only” test

interval, failure occurs in the rock matrix and is governed by the MW criterion ($\sigma_{1rf} = 50$ [kN/m²]).

β_{\min} and β_{\max} can be evaluated from the following formula, by replacing τ_f by $\tau_{rf} = 22.5$ [kN/m²] (see [3]):

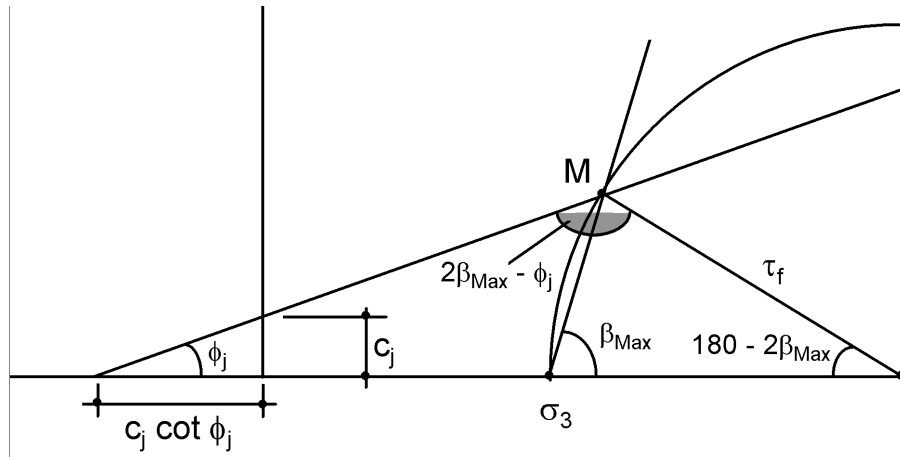


Figure 3.3: Graphical calculation of β_{\max}

$$\tau_\phi = \frac{\sin \phi_j (c_j \cot \phi_j + s_3)}{\sin(2\beta - \phi_j) - \sin \phi_j} \quad (3.1)$$

We find $\beta_{\max} = 80.6^\circ$ and $\beta_{\min} = 29.4^\circ$.

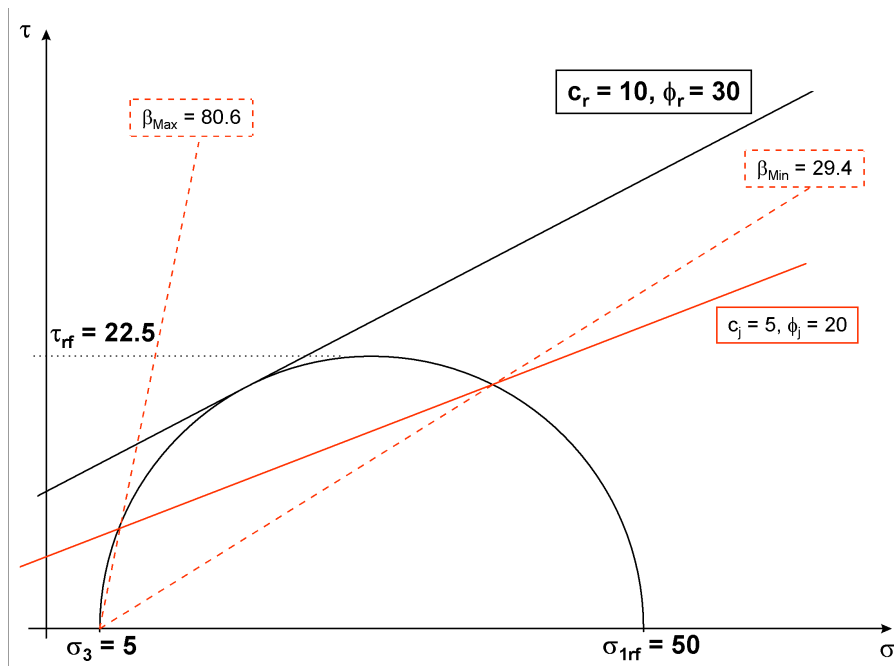


Figure 3.4: Mohr circle for the test with one set of joints

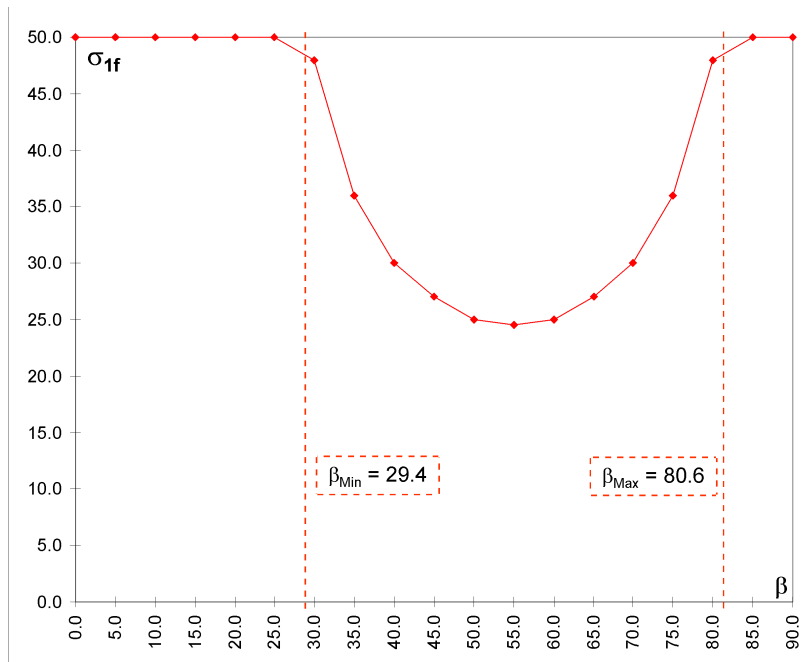


Figure 3.5: $\sigma_{1f} = f(\beta)$ – 2D case

3.2 One element test, two sets of joints, 3D case

The same kind of test is now performed in 3D with two sets of joints. The material characteristics are:

Rock characteristics: $c_r = 10$ [kN/m²], $\phi_r = 30^\circ$ (Drucker-Prager specialization of MW, external size-adjustment)

Joint 1 characteristics: $c_{j1} = 5$ [kN/m²], $\phi_{j1} = 20^\circ$, $\psi_{j1} = 0.66\phi_{j1} = 13.33^\circ$

Joint 2 characteristics: $c_{j2} = 12$ [kN/m²], $\phi_{j2} = 5^\circ$, $\psi_{j2} = 0.66\phi_{j1} = 3.33^\circ$

Invoking (3.1), we can estimate the critical angles for both planes:

$$\beta_{\max 1} = 80.6^\circ, \quad \beta_{\min 1} = 29.4^\circ, \quad \beta_{\max 2} = 72.7^\circ, \quad \beta_{\min 2} = 22.3^\circ$$

Figure 7 shows the geometry of this 3D test with the position of the two sets of joints.

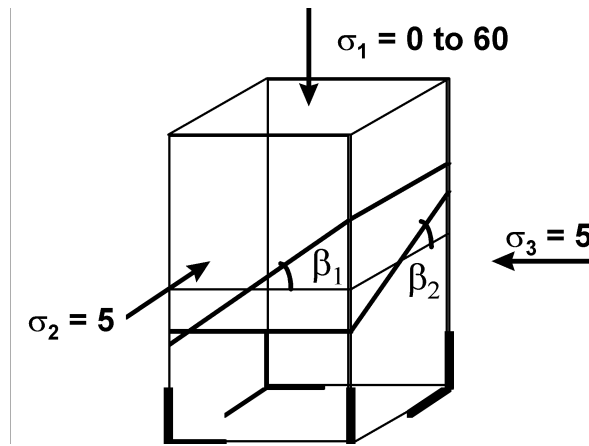


Figure 3.6: One element 3D test, geometry and loading

Four cases are now analysed:

- A. Activation of the first set joint only ($0^\circ \leq \beta_1 \leq 90^\circ$)
- B. Activation of the second set joint only ($0^\circ \leq \beta_2 \leq 90^\circ$)
- C. Activation of both set joints ($\beta_1 = 32.5^\circ$; $0^\circ \leq \beta_2 \leq 90^\circ$)
- D. Activation of both set joints ($\beta_2 = 40^\circ$; $0^\circ \leq \beta_1 \leq 90^\circ$)

Figure 9 shows the results for these cases.

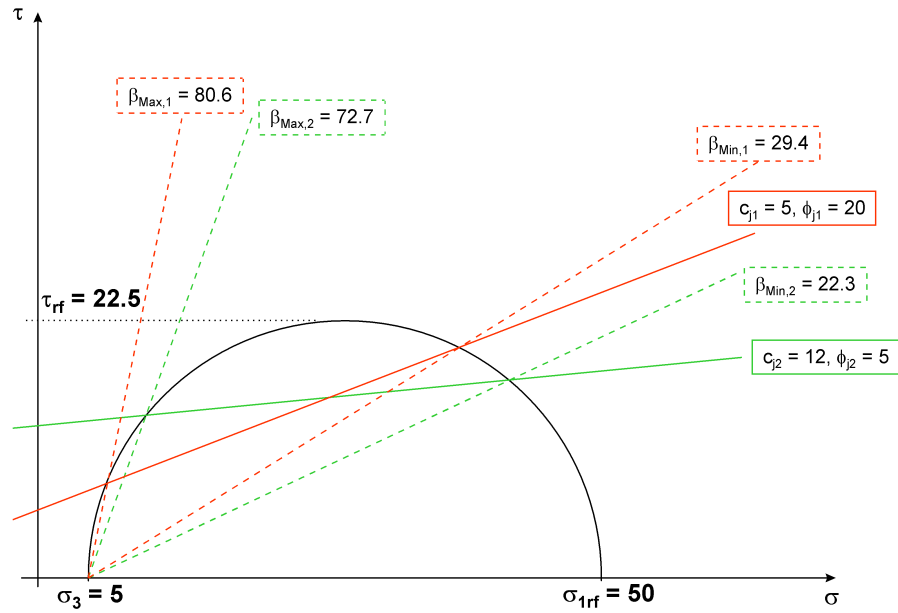


Figure 3.7: Mohr circle for the test with two sets of joints

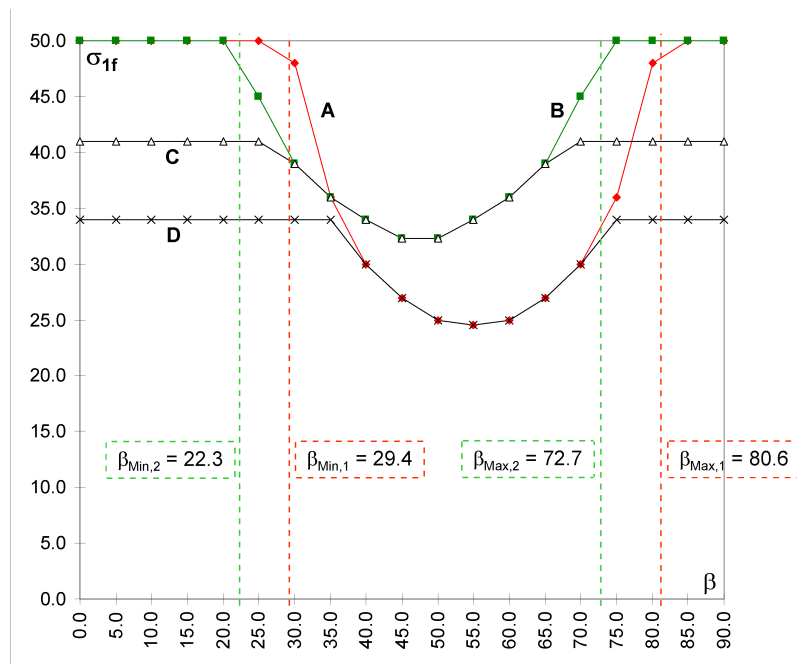


Figure 3.8: $\sigma_{1f} = f(\beta)$ – 3D case

Chapter 4

Applications

4.1 Cuts and slopes

4.1.1 Multilaminate vertical cut

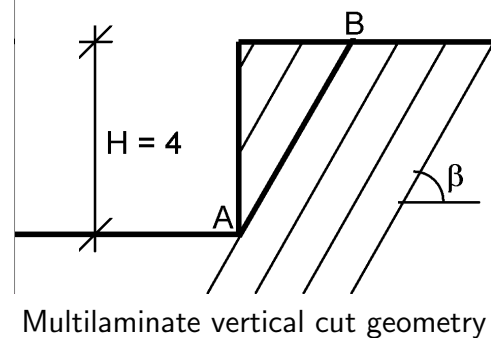
The case of a vertical cut with a single lamina orientation β is considered. The matrix is supposed to be elastic, so that the failure can only occur in the joint.

An approximate analytical solution to this problem can be derived: a shear failure along the weakness plane is expected to take place. The safety factor is estimated as follows:

$$SF = \frac{\int_A^B (s_n \tan \phi_j + c_j) dx}{\int_A^B t dx} = \frac{\tan \phi_j}{\tan \beta} + \frac{2c_j}{gH \sin \beta \cos \beta} \quad (4.1)$$

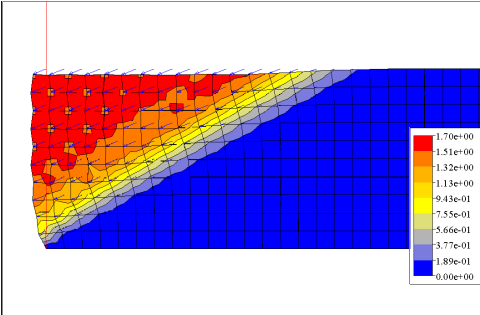
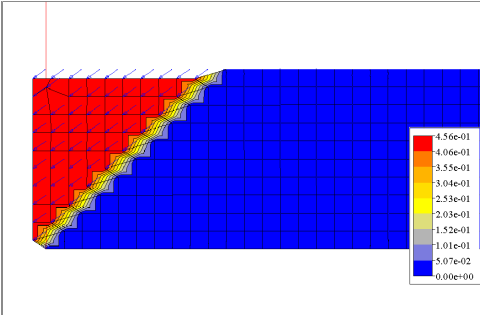
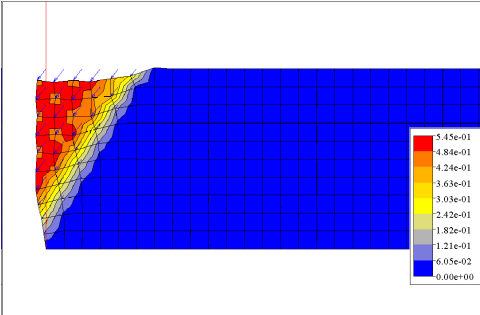
In our case, with the following material parameters and cut geometry:

Rock: $\gamma = 20 \text{ [kN/m}^3\text{]}$, $\nu = 0.3$
 Joint: $c_j = 16 \text{ [kN/m}^2\text{]}$, $\phi_j = 30^\circ$, $\psi_j = 15^\circ$



Results are shown in Table 4.1.

Table 4.1: Results of displacement amplitudes for the multilaminate vertical cut

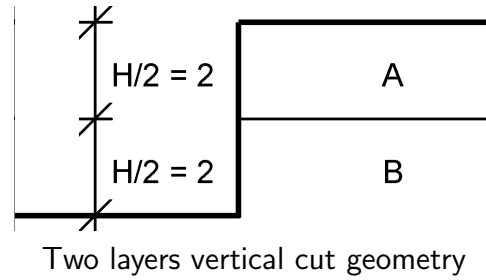
β	SF_{num}	$SF_{Eq. (4)}$	Failure mechanism
30	2.10	1.92	 <p>Failure mechanism for $\beta = 30^\circ$</p>
45	1.40	1.38	 <p>Failure mechanism for $\beta = 45^\circ$</p>
60	1.70	1.26	 <p>Failure mechanism for $\beta = 60^\circ$</p>

Except for very steep lamina angles β , the numerical solution coincides with the approximate solution.

4.1.2 Vertical cut with two layers of material

This test concerns a vertical cut with two layers of material. The geometry and material characteristics are the following:

Layer **A**:
 Rock: $c_r = 4 \text{ [kN/m}^3\text{]}, \phi_r = 20^\circ$
 Joint: $c_j = 4 \text{ [kN/m}^2\text{]}, \phi_j = 15^\circ, \beta = 30^\circ$
 Layer **B**:
 Rock: $c_r = 16 \text{ [kN/m}^3\text{]}, \phi_r = 30^\circ$
 Joint: $c_j = 4 \text{ [kN/m}^2\text{]}, \phi_j = 15^\circ, \beta = 30^\circ$



In this case, as can be expected from examination of stress states on Mohr circles, failure occurs almost simultaneously in both layers. In the top layer A we observe a matrix failure and in the bottom layer B a lamina failure along $\beta = 30^\circ$, as Figure 4.1 shows.

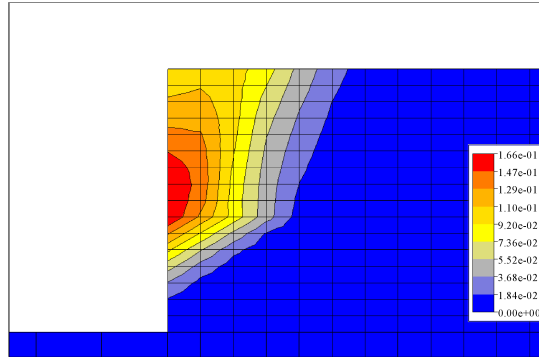


Figure 4.1: Failure mechanism for the “two layers” vertical cut

4.1.3 Slope stability with two sets of joints

The slope stability of a slope with two sets of lamina oriented at $\beta_1 = 52.5^\circ$, and $\beta_2 = 90^\circ$ is analysed next and results are compared with [4].

The simulation starts with an initial state of the unexcavated medium, followed by a simulation of the excavation and finally by a stability analysis.

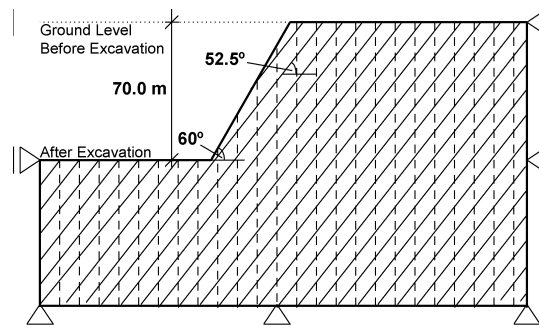


Figure 4.2: Slope stability geometry

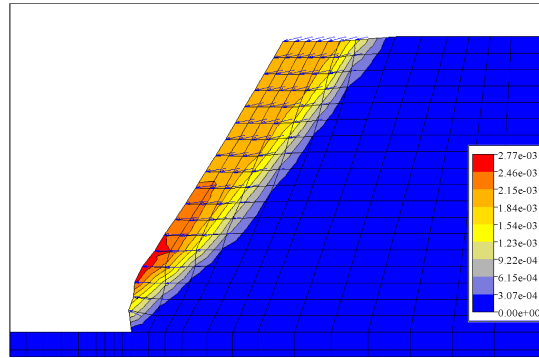


Figure 4.3: Slope stability displacement amplitudes at failure

The material characteristics for both joints are: $c_j = 50$ [kN/m²], $\phi_j = 45^\circ$, while the rock matrix is considered as elastic. Both associated and deviatoric cases have been computed, giving $SF = 1.18$ for $\psi = 0$ and $SF = 1.21$ for $\psi = \phi$, which corresponds to the solution given in [4], although quite different elements and algorithms are being used.

The failure mechanism is illustrated in Figure 4.3.

4.2 Circular hole

The case of a circular hole in an unconfined layered medium is analyzed here. The geometrical and loading setup is shown in Figure 4.4. The medium is initially plain and subjected to a vertical compression. The hole is then excavated and progressively unloaded. Finally, a stability analysis is performed, reducing c and ϕ simultaneously.

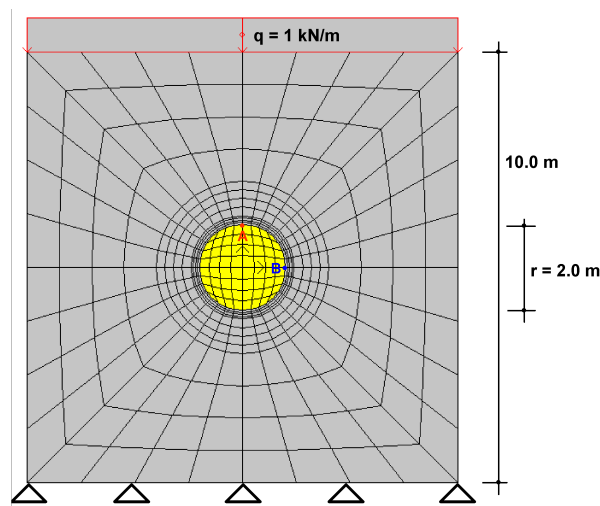
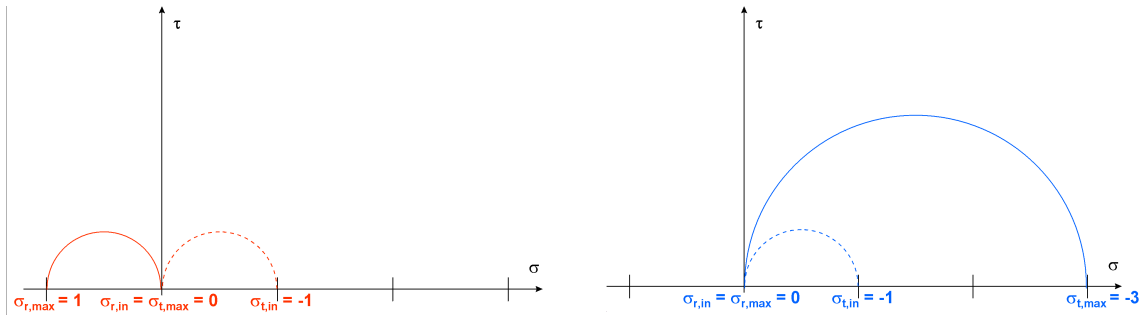
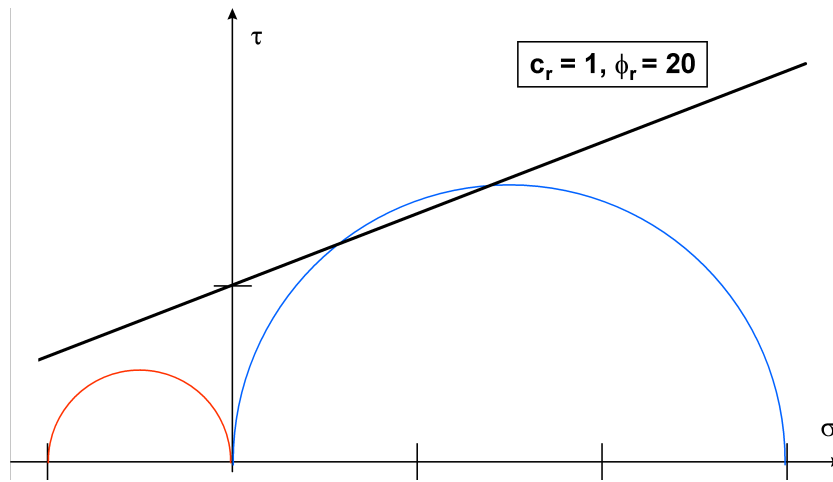


Figure 4.4: Circular hole geometry and loading

The stress evolution at A and B and corresponding Mohr circles can easily be predicted, as illustrated in Figure 4.5. Dotted lines represent the initial configuration, while plain lines represent the final stress state after total unloading. The “ r ” index stands for radial, and the “ t ” for tangential.

Figure 4.5: Mohr circles at point *A* and *B*Figure 4.6: Mohr circle showing moderate plastification at point *B*

Depending on material properties, tensile failure might be initiated at *A* or compressive failure at *B*.

Let us consider the specific case of a Drucker-Prager material defined by $c_r = 1$ [kN/m²], $\phi_r = 20^\circ$, and external size-adjustment on a Mohr-Coulomb criterion. From the corresponding Mohr circle of Figure 4.6, moderate plastification can be predicted at point *B* towards the end of unloading. This is indeed confirmed by the numerical simulation.

If instead we consider a medium constituted by a set of lamina inclined at $\beta = 45^\circ$ ($\beta_{\min} \leq \beta \leq \beta_{\max}$), with properties: $c_j = 0.6$ [kN/m²], $\phi_j = 15^\circ$, $\psi_j = 10^\circ$, and a tension cut-off at $f_t = 0$ (same intact rock properties as before), then plasticity will occur in the lamina about immediately at point *A* and a little bit later at point *B*. This can again be easily read from the corresponding Mohr circles illustrated in Figure 4.7: the Mohr circle illustrating the stress state at point *A* immediately meets the cut-off criterion when translating towards its final position, while the *B* Mohr circle meets the joint criterion about half-way during unloading; Figure 4.8 shows the plastification state at this point.

A stability analysis will then finally lead to a lamina failure illustrated in Figure 4.9a. The same test using a different lamina angle $\beta = 30^\circ$ leads to the failure mechanism shown in Figure 4.9b.

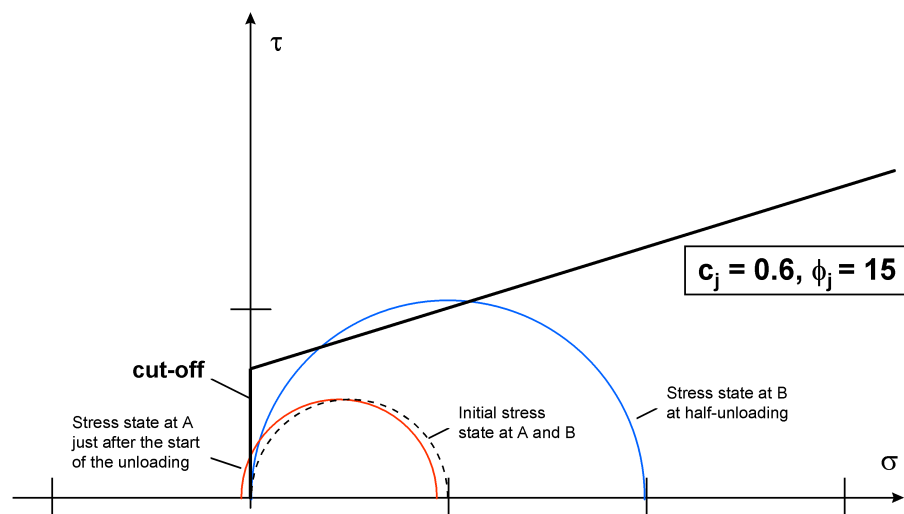


Figure 4.7: Mohr circles at A and B

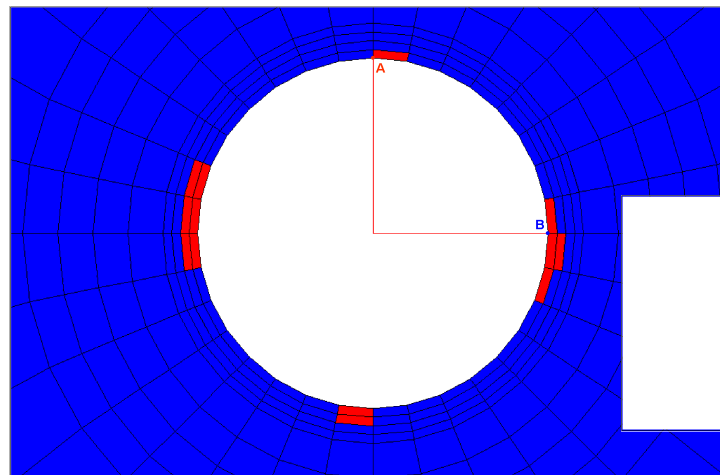


Figure 4.8: Plastification at half-way during unloading

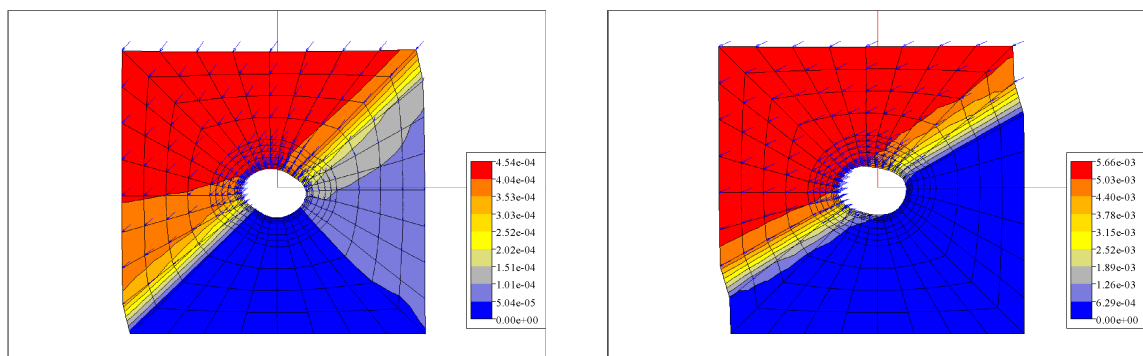


Figure 4.9: Lamina failure for a) $\beta = 45^\circ$ b) $\beta = 30^\circ$

Chapter 5

Conclusion

We describe in this article a modified multilaminate model which takes into account matrix elastoplasticity between weakness planes. The proposed model combines the multilaminate model described in [1] and the general plastic yield surface of Menétrey & Willam [2] and generalizes both.

The model's performance is validated on selected benchmark problems and shows a good correlation with results available for comparison. The proposed model is believed to reproduce more closely the behavior of rock.

References

- [1] Zienkiewicz O.C., Pande G.N. - *Time dependent multilaminate model of rocks* - Int. J. Num. & Anal. Meth. In Geomech., vol. 1, 1977, p. 219–247
- [2] Menétrey Ph., Willam K.J. - *A triaxial failure criterion for concrete and its generalization* - ACI Structural Journal, 92(1), 1995, p. 311–318
- [3] Parry R.H.G. - *Mohr Circles, Stress Paths and Geotechnics*, Ed. E& FN Spon, 1995, p. 81-95
- [4] Sharma K.G., Pande G.N - *Stability of rock masses reinforced by passive, fully-grouted rock bolts* - I.J. Rock Mech. Min. Sci. & Geomech. Abstr. V25, No 5, 1988, p. 273–285.